Modal assurance distribution of multivariate signals for modal identification of time-varying dynamic systems

12 July 2024

Modal assurance distribution of multivariate signals for modal identification of time-varying dynamic systems

Said Quqa[a,*], Luca Landi[a], Pier Paolo Diotallevi[a]

[a] Department DICAM, University of Bologna, Viale Risorgimento 2, 40136 Bologna, Italy

ABSTRACT

Most time-frequency representations (TFRs) and signal analysis methods used for the identification of dynamic systems through non-parametric techniques are based on univariate signals. However, combining the information obtained from different sensors to investigate the overall behavior of the monitored structure is not trivial, as different recordings may show different features. Moreover, methods based upon the analysis of the energy density distribution in the time-frequency plane generally suffer from problems related to crossing and closely-spaced modes. In this paper, a new time-frequency representation of multivariate and multicomponent signals based on the modal assurance criterion (MAC) is presented. The analysis of the modal assurance distribution (MAD) thus obtained enables the extraction of decoupled modal responses, which can then be used to evaluate the instantaneous modal parameters of time-varying systems. To this end, a decomposition algorithm based on modal assurance (DAMA) is proposed, employing the watershed segmentation of the MAD. The results for two case studies, a finite element model and a full-scale experimental benchmark, are shown, considering both the original MAD and two enhanced versions, here proposed to improve its readability. The results are compared with those obtained from modern and widely used techniques, showing the promising efficacy of the proposed method for signals with time-varying frequency and amplitude, even in the presence of narrow-band disturbances and white noise, as well as with vanishing modes.

KEYWORDS: structural health monitoring; time-frequency representation; modal identification; modal assurance; multivariate signal; non-stationary signal.

Declaration of interests: none.

1. INTRODUCTION

Dynamic identification of vibrating systems is a fundamental aspect in different engineering areas, such as civil [1–3], mechanical [4,5], and aerospace [6,7], as it enables the monitoring of dynamic features also for structures which do not show a visible state of degradation, providing information

---

* Correspondence to: Said Quqa, Department DICAM, University of Bologna, Viale Risorgimento 2, 40136 Bologna, Italy, e-mail: said.quqa2@unibo.it

E-mail addresses: said.quqa2@unibo.it (S. Quqa), l.landi@unibo.it (L. Landi), pierpaolo.diotallevi@unibo.it (P.P. Diotallevi).

on their state of health which may support the decision making procedure related to maintenance management or early warning [8].

In the last decades, an increasing number of techniques aimed at dynamic identification have been proposed, attempting to broaden the field of applicability and to release the assumptions which may limit practical applications. Some types of structures are indeed time-varying and traditional identification algorithms based on the assumption of stationarity may be unsuitable. This is generally the case for bridges with vehicular traffic [9], time-periodic systems [10], and robotic or aerospace structures with time-varying geometry [11,12], to name a few.

Also, some research [13–15] has been recently conducted on methods that refer to short-term recordings obtained during strong events (e.g., seismic events) in order to study the variations of structural parameters due to non-linearities. It may therefore be of interest to accurately identify the dynamic parameters and their variations over time, which could be due both to ongoing damage and varying environmental or operational conditions.

For this reason, a large amount of methods has been proposed for the modeling and analysis of non-stationary signals, which can be mainly classified into parametric and non-parametric methods. The first are mainly based on parametrized time series representations, namely, the time-dependent extensions of autoregressive moving average (TARMA) [9,16,17]. On the other hand, the majority of non-parametric methods are based upon time-frequency representations (TFRs) of the vibration energy and allow a more intuitive extraction of modal parameters (i.e., natural frequencies, modal shapes, and damping ratios), which are the most used for damage identification of civil structures due to their explicit physical interpretation [1].

Due to the interconnections born in the last few decades between the fields of linear algebra and subband coding, which in fact are seen as two parts of a single framework [18], a considerable number of transforms leading to different TFRs have been proposed. The short-time Fourier transform (STFT) [19] and the wavelet transform (WT) [20] are among the most used linear transforms; the first employs a fixed complex exponential windowing function for the analysis, while the second relies on a family of more flexible functions. More recently, the S-transform [21] has received extensive interest due to its versatility, since its windowing function is a Gaussian-windowed complex exponential, the dimensions of which scale as a function of frequency, resulting in a frequency-dependent resolution analysis.

The Wigner-Ville distribution (WVD) [22,23] has also been widely studied because of its paramount importance in TFR theory since it does not use any further windowing function except for the signal itself, which is autocorrelated in the transform definition. On the other hand, for this transform, practical applications on multi-component signals are challenging because of its bilinear structure that creates cross-terms which undermine the distribution readability.

Most of the identification methods based on the analysis of TFRs may suffer from problems related to closely-spaced, vanishing, and crossing modes. Furthermore, energy concentrations in the time-frequency (or time-scale) plane could also be due to narrow-band disturbances in the excitation, which would be identified, in most cases, as structural modes.

Two classes of methods aimed at improving the readability of TFRs are reassignment (or reallocation) and synchrosqueezing, shown to be the second a special case of the first [24]. From these post-processing techniques, highly localized TFRs have been derived from STFT and WT. In particular, the synchrosqueezed transform (SST) has been formalized as the application of synchrosqueezing on scalograms obtained through continuous wavelet transform and received great interest as an alternative to the Empirical Mode Decomposition (EMD) [25]. This last method is a completely different technique used to extract signal components associated with

different frequencies, i.e., intrinsic mode functions (IMFs), without relying on any basis function [26], as it happens instead in STFT and WT. It is especially used together with the Hilbert transform (HT), resulting in the Hilbert-Huang transform (HHT). In its original form, this method is however affected by several problems, including mode mixing, which is one of the most important for applications aimed at structural health monitoring (SHM) [27]. For this reason, several variants have been proposed. One of the most used is the ensemble empirical mode decomposition (EEMD), which consists of sifting an ensemble of signals obtained by adding different white noise sequences to the original data and computing the final result as the mean of IMFs obtained [28]. This method still presents issues related to crossing and vanishing modes.

Recently, the concept of modulated multivariate oscillations has been introduced [29,30], together with analysis methods capable of extracting TFRs from multichannel signals, exploiting the inter-channel dependencies which may arise for multivariate data. Namely, extensions to the WVD [31], SST [32] and EMD [33] have been proposed.

In particular, the purpose of multivariate empirical mode decomposition (MEMD) is that of extracting common IMFs from all data sets by analyzing different projections of the multivariate signal in order to calculate its envelopes and local mean. Furthermore, some techniques merge noise-assisted and multivariate approaches into increasingly complex methods [34]. The main disadvantage of these techniques is related to the high computational burden, given by the high number of ensembles necessary to remove the traces of noise introduced in the noise-assisted methods and the number of projections considered in the case of multivariate analysis through MEMD [35].

Except for EMD and its extensions which directly provide IMFs, non-parametric methods require post-processing procedures to extract the modal parameters from TFRs, generally involving the preliminary decomposition into different modal responses [36,37]. To this aim, in several applications, a ridge extraction is directly performed on the TFR by finding the local maxima of the distribution over time [38,39]. This procedure may however suffer by problems related to the presence of components with non-stationary amplitudes and noisy signals [40]. Wang et al. [41] proposed a dynamic optimization method through the introduction of a penalty function for noisy signals, while other authors investigated the use of singular value decomposition (SVD) for ridge detection [42,43]. Ditommaso et al. [13] proposed an algorithm based on the manual selection of the areas of the TFR associated with the modal response of interest, facilitated by the good readability obtained through the S-transform. Quqa et al. [44] proposed an algorithm for near-real-time extraction of modal responses suitable for wireless smart sensing nodes in a decentralized topology, based however on a static filter bank which is updated only at the occurrence of particular situations in order to preserve battery life. This algorithm has been applied in [45,46] for instantaneous damage identification.

After detecting and extracting the ridges, modal parameters can be estimated from the skeleton of the TFR (i.e., the sequence of transform coefficients associated with the ridge) [36]. However, the mere extraction of coefficients associated with the frequency peaks may lead to problems related to the complete reconstruction of decoupled modal responses.

In order to limit these issues, more sophisticated techniques based on image processing applied to TFRs are taking a step into system identification. Some research has firstly employed image processing to de-noise TFRs [47] and to attenuate cross-terms of WVD [48]. Successively, it has also been used to separate modal components. In [49], the regions of the time-frequency plane associated with the energy peaks of different modes are extracted by means of the watershed transform, which is a morphological-based segmentation algorithm [50] previously used by

Roueff et al. on scalograms to separate seismic waves [51]. Zhuang et al. used a simpler 4-connected-component labeling algorithm [52] to decompose the signal in the time-frequency domain [53]. One of the major problems related to these procedures concerns the difficulty of effectively separating closely-spaced modes, which may be merged into the same region of the time-frequency distribution by the pre-processing mathematical morphology operations performed to obtain a proper segmentation (e.g., dilation and closing) [54]. Other issues may arise in the case of noisy signals, for which the energy is spread throughout the time-frequency plane and spurious peaks may be detected.

In this paper, a new representation for multivariate signals based on the modal assurance criterion (MAC) is proposed. In particular, after decomposing all the channels of a multivariate signal into narrow-frequency-band components through the wavelet packet transform (WPT), the wavelet coefficients obtained for consecutive components are interpreted as instantaneous operational deflection shapes (ODS) and compared through the MAC at each time instant. The MAC values are thus reported on the time-frequency plane, where the frequency is given by the index of the wavelet component. As a result, areas with high MAC values (i.e., close to 1) indicate the presence of consecutive components with similar ODSs. Assuming that each signal channel is also affected by uncorrelated white noise, in the regions of time-frequency plane where no vibration mode is excited, MAC values will be randomly distributed between 0 and 1.

The modal assurance distribution (MAD) obtained in this way provides an intuitive representation of the modal features of multivariate signals. Moreover, the method proposed provides a TFR that is not directly dependent on the amplitude of signal components, but only on the signal to noise ratio (SNR) which affects the quality of the evaluated ODS, making it particularly suitable for non-stationary signals, even with vanishing components.

Section 2 describes the proposed method in detail. Here, two techniques aimed at improving the readability of the distribution are also presented. In particular, an averaging criterion between the newly-estimated parameters and the "history" is examined, together with a noise-assisted variant of the procedure.

In Section 3 a decomposition algorithm based on modal assurance (DAMA) is proposed. The algorithm computes the watershed segmentation of the MAD, allowing the extraction of the wavelet coefficients related to different vibration modes and the reconstruction of decoupled modal responses. In addition, some criteria aimed at assessing the effectiveness of decomposition are indicated, analyzing the properties of extracted modes and residue.

In Section 4 two applications of the DAMA are reported. First, a synthetic signal is considered, representing the response of a simply-supported beam with time-varying features. Then, the structural response of a reinforced concrete (RC) structure under progressive damage scenarios is analyzed, performing instantaneous modal identification.

At the end of the paper, concluding remarks are reported, with comments on the most important results obtained by means of the methods proposed.

2. MODAL ASSURANCE DISTRIBUTION

The MAC is one of the most used statistical indicators of the similarity between two different modal shapes. It has been largely employed for identification purposes, in order to compare the results obtained through different techniques [55], to guide the stabilization of stochastic methods [56], and to merge signal components related to the same mode, as in the enhanced frequency domain decomposition (EFDD) [57]. While in the first examples it has been applied to identified modal shapes, in the last case it is used to compare the operating deflection shapes (ODSs) associated with consecutive frequency values. Since EFDD is an identification method in the frequency domain, it does not allow the identification of non-stationary systems. However, the concept of ODS comparison and clustering is extended in this study taking into account the time dependence of modal features, giving rise to the modal assurance distribution (MAD).

2.1 Estimation of the instantaneous ODSs
The displacement response in space and time $u(z,t)$ of a linear structure with distributed mass and elasticity in the continuous time, excited by a generic forcing function, can be represented in general as [58]:

$$u(z,t) = \sum_{j=1}^{\infty} \phi_j(z) q_j(t) \tag{1}$$

with $\phi_j(z)$ the continuous j-th modal shape and $q_j(t)$ a function of time with narrow (in general, depending on damping) frequency band, the center of which is the damped frequency $\omega_{d,j}$.
Considering a structure with slowly varying features (i.e., with masses and stiffness which are assumable as piece-wise constant), the discrete signal recorded at a given position i by means of a uni-axial accelerometric sensor can thus be modeled as:

$$x_i[t] = \sum_{j=1}^{\infty} \phi_{i,j}^{(t)} \ddot{q}_j[t] + v_i[t] \tag{2}$$

where $\phi_{i,j}^{(t)}$ is the piece-wise constant element of the j-th modal shape, $\ddot{q}_j[t]$ is the double derivative in time of $q_j[t]$, and $v_i[t]$ represents a white noise function referring to the i-th sensor. Applying a band-pass filter with impulse response $b_k[t]$ to the recorded signal $x_i[t]$, the filtered structural response can be computed as:

$$(x_i * b_k)[t] = \sum_{j=1}^{\infty} \phi_{i,j}^{(t)} (\ddot{q}_j * b_k)[t] + (v_i * b_k)[t] \tag{3}$$

because of the linearity of the convolution operator (here indicated as $*$). Since $q_j[t]$ has a narrow band in the frequency domain, the terms of summation which give a non-zero result are only those with $\omega_{d,j}$ close to the frequency band of b_k, i.e., $(\ddot{q}_j * b_k)[t]$ is different from an all-zeros sequence only if $Q_j(\omega)B_k(\omega) \neq 0$ for some value of ω, where $Q_j(\omega)$ and $B_k(\omega)$ denote the

Fourier transforms of $\ddot{q}_j[t]$ and $b_k[t]$, respectively. Indicating with $q_k[t]$ the time function with frequency $\omega_{d,k}$ included within the cutoff frequency values of $b_k[t]$ and neglecting the contributions of neighboring modes, the filtered response can be rewritten as:

$$x_{i,k}[t] \cong \phi_{i,k}^{(t)}(\ddot{q}_k * b_k)[t] + v_{i,k}[t] \tag{4}$$

with $x_{i,k}[t] = (x_i * b_k)[t]$ and $v_{i,k}[t] = (v_i * b_k)[t]$. Considering moreover the signal $x_r[t]$ collected at a reference sensor position r, the instantaneous ratio between $x_{i,k}[t]$ and $x_{r,k}[t]$, obtained as indicated in (4) through the same filter $b_k[t]$, is:

$$\frac{x_{i,k}[t]}{x_{r,k}[t]} \cong \frac{\phi_{i,k}^{(t)}(\ddot{q}_k * b_k)[t] + v_{i,k}[t]}{\phi_{r,k}^{(t)}(\ddot{q}_k * b_k)[t] + v_{r,k}[t]} \tag{5}$$

If the k-th vibration mode is sufficiently excited, the noise terms become negligible, and an estimate of the i-th element of the instantaneous modal shape can be calculated as:

$$\phi_{i,k}[t] \cong \gamma_k^{(t)} \frac{x_{i,k}[t]}{x_{r,k}[t]} \tag{6}$$

with $\gamma_k^{(t)} = \phi_{r,k}^{(t)}$ representing an instantaneous normalization factor. Considering a multivariate signal consisting of the accelerations collected at different sensor locations, the instantaneous modal shapes can be obtained by normalizing all the estimated values with respect to the same position.

Considering a filter with impulse response $b_{\bar{k}}[t]$ such that none of the natural frequencies are included between its cutoff frequencies, all the terms in the summation of Equation (3) are close to zero and may thus be neglected, with the filtered signal becoming:

$$x_{i,\bar{k}}[t] \cong v_{i,\bar{k}}[t] \tag{7}$$

and consisting of a filtered noise component. Therefore, the ratio between $x_{i,\bar{k}}[t]$ and $x_{r,\bar{k}}[t]$ continuously varies over time without reflecting the structural behavior.

2.2 Signal-adaptive extension of the MAC

In the original formulation, the MAC is defined as a normalized scalar product of two vectors $\boldsymbol{\varphi}_a$ and $\boldsymbol{\varphi}_b$ representing two complex modal shapes or ODS:

$$MAC_{a,b} = \frac{|\boldsymbol{\varphi}_a^T \boldsymbol{\varphi}_b^*|^2}{(\boldsymbol{\varphi}_a^T \boldsymbol{\varphi}_a^*)(\boldsymbol{\varphi}_b^T \boldsymbol{\varphi}_b^*)} \tag{8}$$

where $\boldsymbol{\varphi}^*$ represents the complex conjugate and $\boldsymbol{\varphi}^T$ the transpose of $\boldsymbol{\varphi}$. In this study, the concept of modal assurance is applied to instantaneous estimates of the ODSs, calculated using narrow-frequency components of the signals collected at different locations, obtained by means of the WPT, as schematized in Fig. 1.
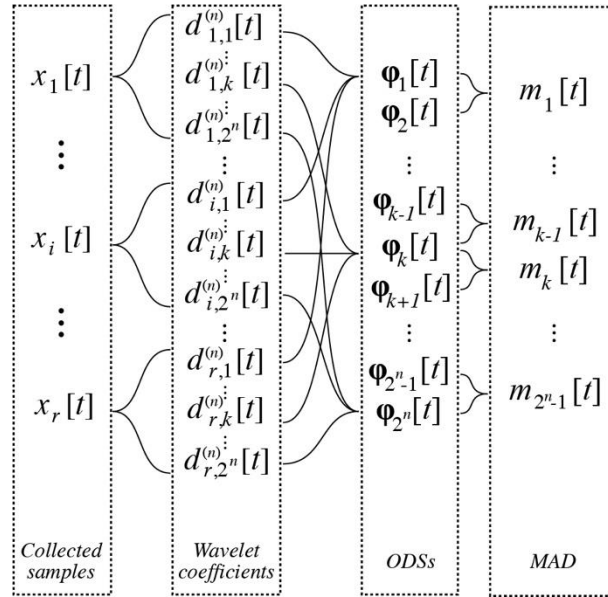
Fig. 1: Schematics of MAD

Considering a complete decomposition tree, the wavelet packet coefficients $d_{i,2k}^{(p+1)}[t]$ and $d_{i,2k+1}^{(p+1)}[t]$ obtained by decomposing the coefficients $d_k^{(p)}$ at the level p can be calculated recursively through the Mallat algorithm [59] as:

$$d_{i,2k}^{(p+1)}[t] = d_k^{(p)} * \bar{h}[2t]$$

$$d_{i,2k+1}^{(p+1)}[t] = d_k^{(p)} * \bar{g}[2t] \tag{9}$$

where $k = 0, \dots, 2^p$ indicates the subband of the obtained coefficients, $*$ denotes the convolution operator, and $h[t] = \bar{h}[-t]$ and $g[t] = \bar{g}[-t]$ are the impulse responses of the low-pass and high-pass filters associated with the selected wavelet function, respectively. Considering the discrete signal $x_i[t]$ collected at location i, the root of the tree $d_0^{(0)}[t]$ can be assumed coincident with $x_i[t]$ if the sampling frequency of the collected signal is sufficiently high, committing however a "wavelet crime" [60]. It should be noted that the wavelet decomposition can also be implemented as a filtering procedure using a filter bank the elements of which are 2^n equivalent filters that produce the coefficients (9) at the final transformation level, say n [18]. Each filter obtained through this procedure has a passband range of $F_s/2^{n+1}$, where F_s is the sampling frequency of the collected signal. It should be noted that, at a given transform level, a higher sampling frequency determines filters with wider passband range. It is therefore essential, in the case of high sampling frequencies, to select transforms with higher level to obtain a good frequency discretization of the signal. However, the maximum selectable level depends on the length of the signal and on the filter order. In particular, it is equal to the integer number $n_{max} \le \log_2(N/N_f)$, where N and N_f are the length of the signal and the order of the filter associated with the mother wavelet, respectively.

The terms of vector $\boldsymbol{\varphi}_k[t]$, representing the real normalized instantaneous ODSs associated with a given subband k of the level n can thus be computed through the ratio:

$$\varphi_{i,k}[t] = \frac{d_{i,k}^{(n)}[t]}{d_{r,k}^{(n)}[t]} \tag{10}$$

with $d_{i,k}^{(n)}[t]$ denoting the t-th sample of the wavelet component related to the subband k obtained by decomposing the signal collected at the location i, and r indicating a reference location. Using these instantaneous estimates, the MAD is defined as the matrix $\mathbf{M}_{[2^n-1 \times T]} = \left[\mathbf{m}[0], \mathbf{m}[1], \dots \mathbf{m}[T]\right]$ consisting of the $\mathbf{m}[t]$ vectors, related to time instants t, containing the elements:

$$m_k[t] = \frac{\left|\boldsymbol{\varphi}_k^{\mathrm{T}}[t]\boldsymbol{\varphi}_{k+1}[t]\right|^2}{(\boldsymbol{\varphi}_k^{\mathrm{T}}[t]\boldsymbol{\varphi}_k[t])(\boldsymbol{\varphi}_{k+1}^{\mathrm{T}}[t]\boldsymbol{\varphi}_{k+1}[t])} \tag{11}$$

with $k = 1, \dots, 2^n - 1$ and T denoting the length of $d_{i,k}^{(p)}$. Each element of $\mathbf{M}$ assumes a value between 0 and 1 and represents the instantaneous similarity of ODSs related to neighboring components k and $k + 1$. The ability to represent the time-varying modal features of the analyzed signal is due to the fact that damped modes have values in the frequency spectrum which are spread around the peak represented by the damped frequency. The spreading is generally dependent on both damping and natural frequency of the selected mode. If a sufficiently high decomposition level n is selected for analyzing the response of a damped structure, the part of the spectrum related to each mode is divided into a set of narrow-frequency band components. Each of these components is however part of the same mode and, therefore, have similar ODSs (calculated by considering the same components of signals collected at different locations). This fact leads to high MAD values in the regions of the time-component plane where subbands of the same mode are present. On the other hand, the signal filtered through cutoff frequencies selected far from the damped frequency values consists of a filtered noise component, as reported in Equation (7), thus not characterized by physically meaning features which would generate persistently high MAD values in the time-component plane.

2.3 Methods to improve the readability
Far from natural frequencies, high MAD values are generated by random similarities between the ODSs of neighboring filtered noise components. This phenomenon may compromise the readability of the distribution and prevent a correct application of procedures for the extraction of modal responses. In order to reduce this risk, two techniques are proposed in this section to improve the readability of MAD.
The first involves the selection of a forgetting factor α, used to compute the t-th element of a weighted distribution that also takes into account the previous estimates. In particular, each element of the weighted distribution $\bar{m}_k[t]$ can be computed as:

$$\bar{m}_k[t] = (1 - \alpha)m_k[t] + \alpha\bar{m}_k[t - 1] \tag{12}$$

The higher is α and the more the distribution appears smooth in the time direction, resulting however in a slower updating and a lower sensitivity to sudden variations. This method is particularly effective to remove noise-generated random similarities, which are generally characterized by sharp peaks with short duration in time.

The second criterion consists of a noise-assisted approach which, similar to the concept used in the EEMD, involves the computation of the final MAD as the mean of an ensemble of L matrices, each consisting of the MAD evaluated on the multivariate signal plus an uncorrelated finite-amplitude white noise matrix. Operating in this way, only persistently high values over the ensemble of trials will form the high-similarity areas of the final MAD, canceling out spurious peaks due to noise components which are different for each trial. The ensemble MAD is computed as:

$$\widetilde{m}_k[t] = \frac{1}{L} \sum_{\lambda=1}^{L} m_k^{(\lambda)}[t] \tag{13}$$

where $m_k^{(\lambda)}[t]$ is the MAD value obtained on the λ-th noise-added trial $\mathbf{x}[t] + \mathbf{v}_\lambda[t]$, with $\mathbf{x}[t] = \left[x_1[t], x_2[t], \dots, x_r[t]\right]^{\mathrm{T}}$ the collected multivariate signal and $\mathbf{v}_\lambda[t] = \left[v_{\lambda,1}[t], v_{\lambda,2}[t], \dots, v_{\lambda,r}[t]\right]^{\mathrm{T}}$ a vector of uncorrelated white noise sequences. In order to prevent the added noise from covering the signal parts with low amplitude, the $v_{\lambda,k}[t]$ sequences can be chosen as non-stationary, having amplitude dependent on the analyzed signal:

$$v_{\lambda,k}[t] = \beta \, std\{x_k[t - \tau, t + \tau]\} \, s_{\lambda,k}[t] \tag{14}$$

with $std\{x_k[t - \tau, t + \tau]\}$ denoting the standard deviation of x_k in the interval from $t - \tau$ to $t + \tau$, $s_{\lambda,k}[t]$ is a sequence of zero-mean white noise with standard deviation 1, and β, τ are user-defined parameters that control the amplitude and adaptivity of the added noise, respectively. Considering the wavelet filters as ideal bandpass filters, if β is higher than the standard deviation of the recording noise and the ensemble is formed by a high number of trials, the mean of MAD values in noise-only areas can be estimated as $1/r$, where r is the number of sensors. It is indeed easy to prove that the expected value of the normalized dot product between two vectors $\mathbf{a}, \mathbf{b} \in \mathbb{R}^N$, the elements of which are random variables independently distributed in a given interval, is:

$$\mathrm{E}\left[\frac{|\mathbf{a} \cdot \mathbf{b}|^2}{|\mathbf{a}|^2 |\mathbf{b}|^2}\right] = \frac{1}{N} \tag{15}$$

Since wavelet filters with limited order cannot be considered as ideal bandpass filters, the filtered noise components cannot be assumed as independent. Especially for high transform levels, the expectation of MAC tends in fact to a value which is higher than $1/r$. This value becomes however the minimum of MAD, canceling out the effects of recording noise.

The criteria proposed here can also be applied together, increasing the readability of the distribution at the expense of a higher computational burden.

3. DECOMPOSITION ALGORITHM BASED ON MODAL ASSURANCE

The MAD can be used as a TFR for visualizing the distribution of modal features through the time-component plane (from now on, mentioned as time-frequency plane, since the conversion is straightforward). Moreover, it can also be exploited to separate modal responses, since the physical meaning of the distribution enables the construction of a set of adaptive bandpass filters which allows the extraction of separate signal components delimited by low-valued MAD areas.

3.1 Outline of the decomposition algorithm

In order to automatize the recognition of the areas representing different modes, an algorithm based on watershed segmentation and MAC-based cluster analysis is proposed in this section. In this algorithm, the MAD is interpreted as a grey-scale image obtained by assigning the color white to 1 and black to 0 values. A mask $\boldsymbol{\Xi}_{[2^n-1 \times T]}$ is then created, able to select the MAD values above a user-defined threshold η. Before applying the mask to the grey-scale distribution, opening and filling morphological operations are performed to remove small white peaks and black holes generated by noise.

Then, a Gaussian filter with low standard deviation is applied to the masked matrix $\widehat{\mathbf{M}} = \boldsymbol{\Xi} \cdot \mathbf{M}$ (with $\cdot$ denoting the point-wise multiplication) to further smoothen the distribution, and the local maxima are identified. Finally, the watershed transform is applied to segment the masked distribution into different areas, each containing a single maximum, which are then converted into matrices $\boldsymbol{\Xi}_{a\,[2^n-1 \times T]}$, each with the same size of $\widehat{\mathbf{M}}$, consisting of 1-values in the identified area and 0 values elsewhere.

For each identified area, the a-th signal (localized both in frequency and time) can be extracted by means of a reconstruction matrix $\mathbf{R}_{a\,[2^n \times T]}$, the elements of which are obtained as:

$$\rho_{a,k}[t] = \begin{cases} 1 & if\ \xi_{a,k}[t] = 1 \lor \xi_{a,k-1}[t] = 1 \\ 0 & otherwise \end{cases} \tag{16}$$

where $\xi_{a,k}[t]$ are the elements of $\boldsymbol{\Xi}_a$. The partial multivariate signal component $\mathbf{w}_a[t]$ extracted by $\mathbf{R}_a$ can thus be computed as the inverse wavelet packet transform (IWPT) applied to the masked wavelet coefficients $r_{i,k}^{(n)}[t] = d_{i,k}^{(n)}[t]\rho_{a,k}[t]$. By means of the Mallat algorithm [59], the coefficients $r_{i,k}^{(p)}[t]$ at level p can be evaluated recursively as:

$$r_{i,k}^{(p)}[t] = \check{r}_{i,2k}^{(p+1)} * h[t] + \check{r}_{i,2k+1}^{(p+1)} * g[t] \tag{17}$$

where $\check{r}[t]$ indicates the sequence obtained by inserting a zero between each sample of $r[t]$. Therefore, $w_{i,a}[t] = r_{i,0}^{(0)}[t]$ represents the i-th element of $\mathbf{w}_a[t]$ (i.e., referring to the i-th sensor location).

After reconstructing the partial components, each of them can be associated with a vibration mode by performing a MAC-based clustering procedure. In particular, the average modal shape of the a-th partial component can be computed as:

$$\boldsymbol{\varphi}_a = \frac{1}{s} \sum_{t=1}^{s} \frac{\mathbf{w}_a[t]}{w_{1,a}[t]} \tag{18}$$

with s the number of non-zero time samples in $w_{1,a}[t]$. Then, the clustering can be performed with the following rule:

$$\boldsymbol{\varphi}_a, \boldsymbol{\varphi}_b \in C_l \Leftrightarrow MAC_{a,b} \geq 1 - \theta \tag{19}$$

where C_l represents the l-th cluster (related to the l-th mode), $MAC_{a,b}$ is the modal assurance value between the shapes $\boldsymbol{\varphi}_a$ and $\boldsymbol{\varphi}_b$ obtained using two partial components $\mathbf{w}_a$ and $\mathbf{w}_b$, respectively, while θ is a user-defined sensitivity parameter.

The complete decoupled modal responses can thus be obtained by merging (i.e., summing up) all the partial components associated with the same cluster. Moreover, instantaneous modal parameters can be identified from the extracted mono-component responses using, for example, the HT or the Teager energy operator (TEO) [44]. In particular, the responses extracted in locations far from the nodes of the modal shapes should be used to retrieve instantaneous frequencies in order to limit the influence of noise in their evaluation.

In a previous work [44], the authors presented a two-step procedure for decoupling structural responses through clustered filter banks (CFBs) onboard wireless smart sensor networks. In the mentioned paper, the CFBs employed for decomposition are generated at the beginning of the procedure and used until the occurrence of particular events (e.g., damage or strong environmental variations) that make the filters no more suitable for modal identification due to their fixed cutoff frequencies. It should be noted that the DAMA proposed in the present paper is equivalent to a band-variable filter bank the parameters of which are signal-adaptive and estimated upon the MAD. This generalized filter bank with a variable number of components and cutoff frequencies enables the automatic extraction of modal responses even at the occurrence of strong variations in the dynamic behavior of the monitored system and in presence of vanishing components.

3.2 Parameter selection and residual analysis

The selection of different values for η and θ may lead to different decompositions. In particular, η is responsible for signal segmentation: the higher this threshold, the smaller the masked areas, which could be eroded during the morphological operations, reducing however the noise included in the reconstructed partial components. On the other hand, θ concerns the final clustering procedure: high values of this parameter lead to more clusters, which could nevertheless belong to the same mode if slight variations affect the modal shapes over time (e.g., due to ongoing damage).

A method for verifying the proper selection of the first parameter consists of the residual analysis. The residual of the DAMA can be obtained as:

$$\boldsymbol{\varepsilon}[t] = \mathbf{x}[t] - \sum_a \mathbf{w}_a[t] \tag{20}$$

The variance of this sequence should be similar to the variance of the recording noise, and therefore low if compared to the variance of the original signal. It is worthy to note that, even by

applying the noise-assisted method, the signal is not affected by added noise, since it is only used to select the masking matrix, which is then applied to the decomposed original signal.

A criterion for selecting the correct value of η in offline implementations could consist of applying DAMA with multiple thresholds, selecting the parameter after observing the curve of residual variance as a function of η. As the threshold increases, the variance of the residual should increase steeply for low and high values of η, presenting a lower slope in the central part. The first interval with a high slope is due to the overcoming of the recording noise, while the second part represents the inclusion of significant signal components into residuals. The optimal value of η should therefore be selected in the part contained between these two high-slope intervals, for example immediately after the first one or where the slope of the curve is minimum.

The θ parameter should be selected in order to obtain a small number of clusters that generate mono-component decoupled responses, i.e., containing information related to a single modal response. A PCA should thus be performed on the modal responses extracted at different sensor locations to evaluate the variance explained by each principal component (PC). In order to be mono-component, the percentage of variance explained by the first PC should be much higher than the variance explained by the others [61]. High variance explained in the other principal directions may denote both multi-component responses and high noise in the recordings. The first involves errors in the estimation of modal parameters for all sensor locations, except for those near to a node of the modal shape of the disturbing mode. On the other hand, if only a subset of recordings is characterized by a low SNR (due for example to the deployment of sensors near to a structural constraint), only the responses extracted at those locations will provide noisy parameters. If multi-component responses are identified, the analysis should be repeated upon increasing the θ parameter.

4. APPLICATIONS

In this section, the MAD is employed to decouple the modal responses of two case studies. The first consists of a simply-supported beam modeled through a finite element software, while the second is a full-scale RC building tested on a shaking table at the University of California, San Diego.

4.1 Case study 1: simulated simply-supported beam

The first case study was modeled as a simply-supported RC beam with a rectangular section (40 cm wide and 85 cm high) and a length of 10 m. The simulated instrumentation consists of four uni-axial accelerometers deployed in the vertical direction, as represented in Fig. 2. Damping with a ratio of 0.02 was selected for each mode to solve the equation of motion and obtain the structural response through the Newmark method. In order to simulate localized time-varying damage, a segment of the structure is modeled with varying Young modulus, as reported in Fig. 3. In particular, the damage is modeled as slowly increasing up to 1400 seconds, when an instantaneous retrofit is simulated.
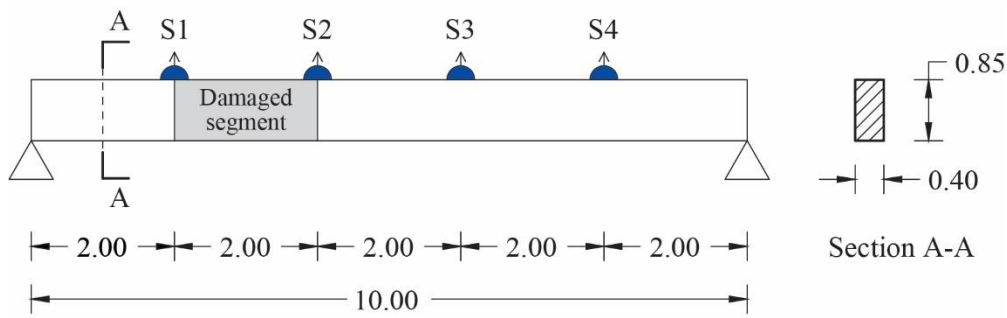
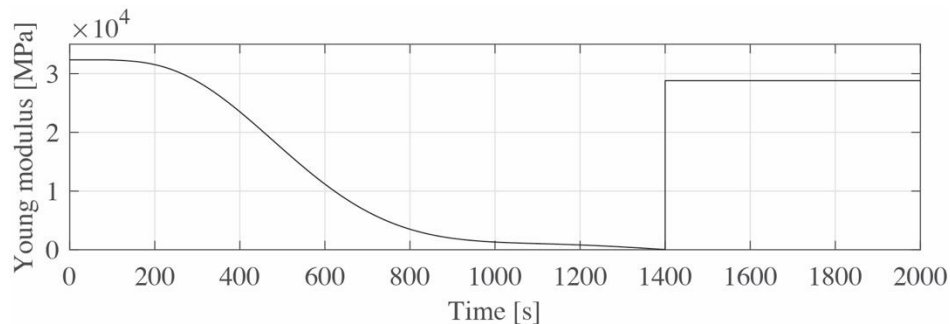*Fig. 2: Scheme of the case study 1, units in meters*

Fig. 3: Simulated damage over time

The data used to compute the MAD consists therefore of a multivariate signal of 2000 seconds, obtained by using the accelerations collected at the sensor locations indicated in Fig. 2 with a sampling frequency of 250 Hz. The input excitation used to compute the structural response is a synthetic acceleration obtained by adding a white noise sequence with a standard deviation of 1 m/s^2 to a harmonic component with amplitude 0.3 m/s^2 and frequency of 50 Hz, which simulates a narrow-band disturbance, as reported in Fig. 4. The exciting input was applied to 11 nodes, equally spaced of 1 m, in the vertical direction. Before using the signals, each collected acceleration sequence was corrupted by introducing a zero-mean white noise component with a standard deviation of 10% with respect to that of the original response.
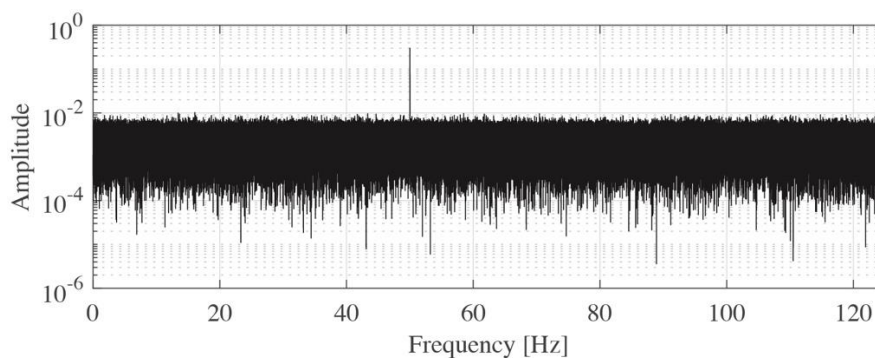
Fig. 4: Frequency spectrum of the input excitation for case study 1

In Fig. 5, the power spectrum of the signal collected at sensor location S3 computed through the STFT is represented. The narrow-band disturbance generates a high-amplitude component that intersects the modal responses in the time-frequency plane. This persistent peak in the frequency

spectrum could be interpreted as a modal component by analyzing the results of most of the traditional structural identification procedures. Moreover, it could corrupt neighboring modes and induce problems related to crossing modes.
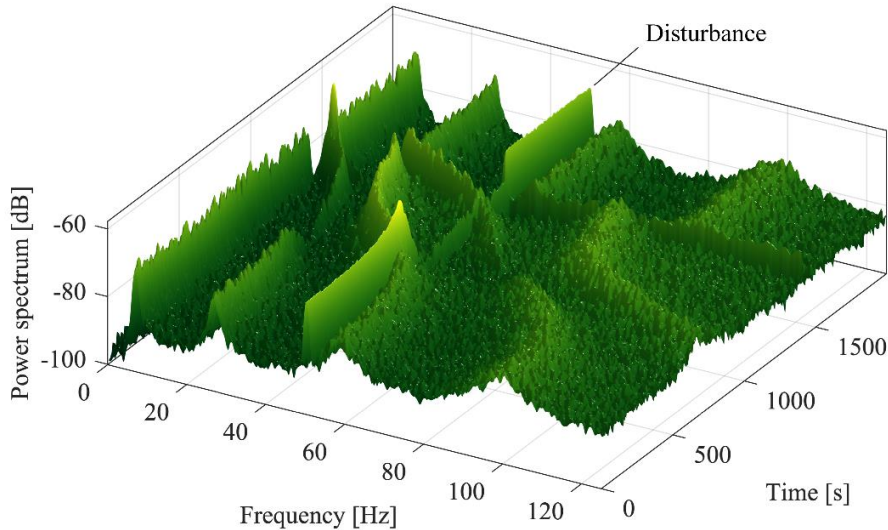

Fig. 5: Power spectrum of the analyzed signal

The MAD was calculated on the multivariate signal by selecting the Fejér-Korovkin 22 wavelet function with a decomposition level 8 (Fig. 6a). In this case, the decomposition bank consists of 256 filters with passband range of 0.49 Hz.

It is possible to observe that regions in the time-frequency plane with high values (in white) are present along the entire distribution, following the trend of damage and also reflecting the abrupt variation that occurs at 1400 s. However, the disturbance component is completely overlooked, resulting in low MAD values around 50 Hz, since the ODSs associated with neighboring subbands are different.

Due to the random similarities in noise-generated ODSs, there is a consistent number of spurious peaks which could undermine the application of DAMA. To smooth the distribution before further analyses, a forgetting factor of 0.9 is adopted, which leaves the frequency resolution unchanged but removes abrupt variations on the time axis, introducing however a slight delay in the updating of the equivalent band-variable filters (Fig. 6b). Afterward, a mask is applied to the distribution selecting the areas with MAD value higher than $\eta = 0.50$. In Fig. 7, the variance of residual is reported in logarithmic scale as a function of η. It is possible to notice that the first interval with a high slope is for threshold values of 0.10-0.30, while other jumps are observable around 0.70 and 0.85. The optimal value was chosen between these two intervals, where the slope of the average curve is minimum.
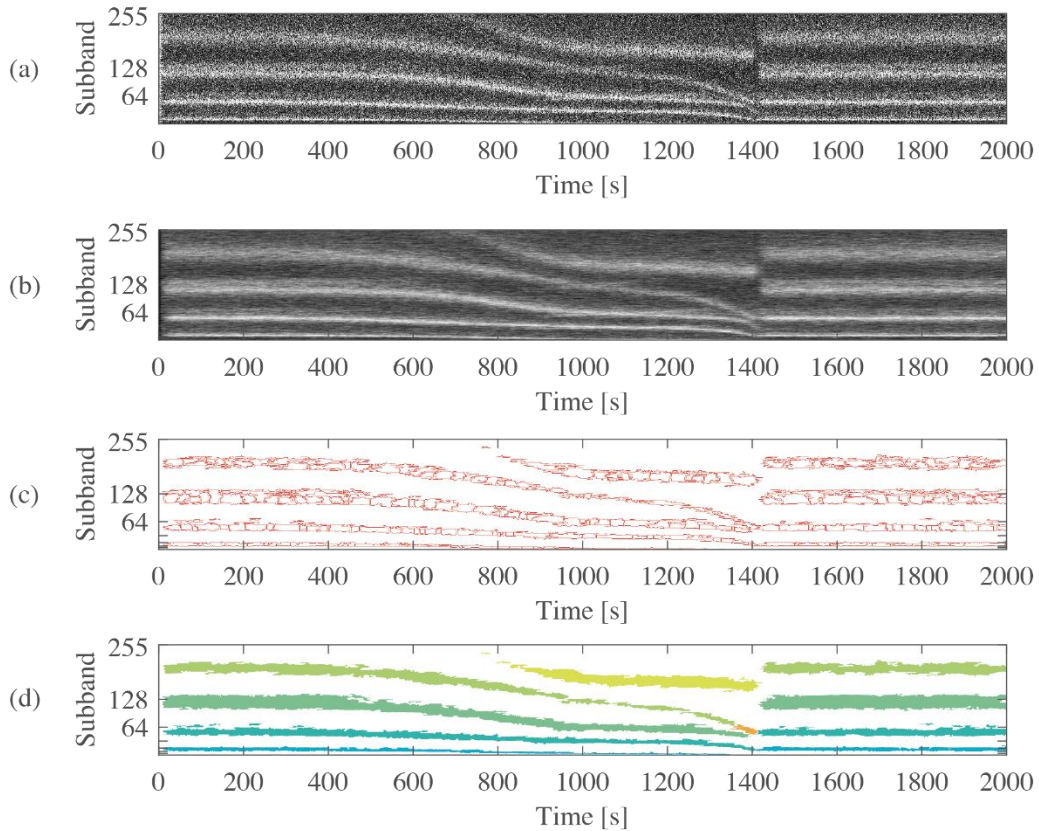
14

Fig. 6: MAD, smoothed MAD, watershed segmentation and DAMA application
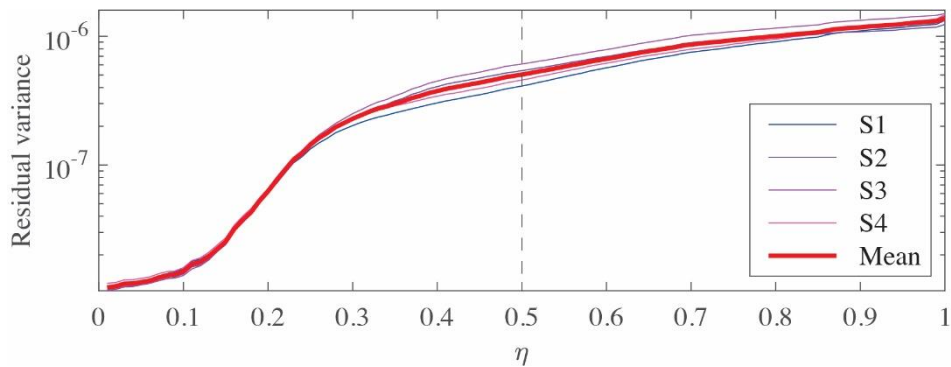

Fig. 7: Residual variance for different values of threshold, case study 1

It is possible to observe how the frequency spectrum of the residual of sensor S4 (Fig. 8) is very similar to that of the input, i.e., almost white, except for the narrowband disturbance at 50 Hz. On the other hand, the spectrum of the reconstructed signal (obtained by summing up all the modal responses extracted at location S4) approximates well that of the original structural response, confirming the fact that all the significant information is extracted from the through DAMA.
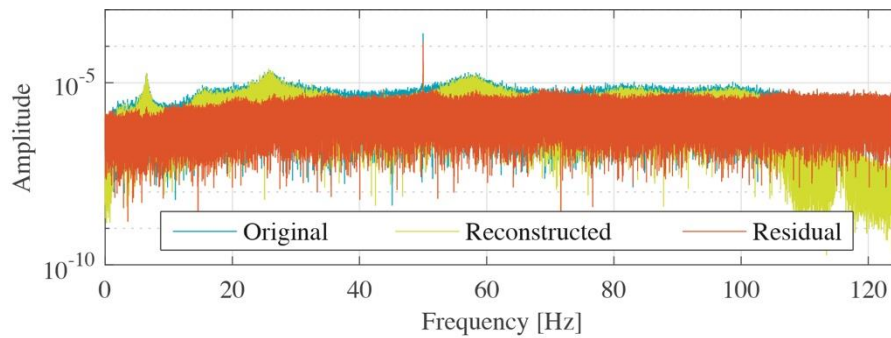
Fig. 8: Frequency spectrum of the residual

In order to apply the watershed segmentation, a Gaussian filter with standard deviation 1 is used before extracting the local maxima and obtaining the areas reported in Fig. 6c.

MAC-based clustering with sensitivity $\theta = 0.05$ is then applied to associate the components obtained by reconstructing the partial signals related to each area to a different vibration mode. In this way, the areas shown in Fig. 6d are obtained. In this experiment, a total number of 6 vibration modes are identified, one consisting of the orange area located around 1400 s, which should however be part of the fourth mode. The missing association with the appropriate cluster is due to the substantial change in the modal shape of mode 4 caused by the highly damaged state at the time interval close to 1400 s.

The instantaneous frequencies identified by applying the HT to the decoupled modal responses extracted by means of DAMA on the signal collected in location S4 are reported in Fig. 9, superimposed on the theoretical values and on the disturbance component. A median filter with a window size of 1000 samples was applied to the identified frequencies before plotting, in order to improve the readability of the figure.
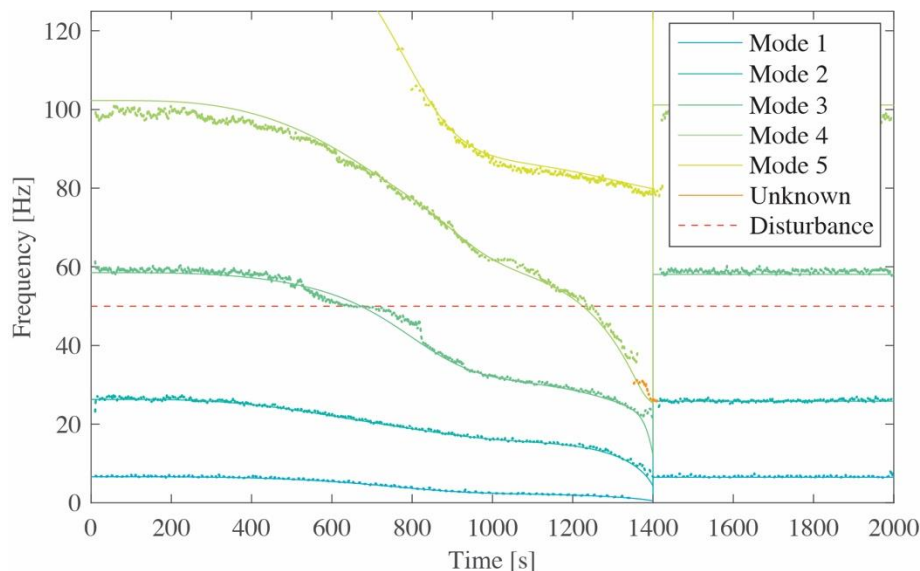

Fig. 9: Theoretical (solid lines) and estimated (dots) instantaneous natural frequencies

The estimated values for the first two modes are almost coincident with the theoretical curves. The third natural frequency is well-identified except for the time interval in which the disturbance intersects the natural frequency curve. On the other hand, the fourth frequency is not influenced

16

by the disturbance, presenting however a slight underestimation for higher frequencies. The fifth mode is vanishing, since it is only visible in the interval between 700 and 1400 s due to the selected sampling frequency. However, a good estimation for the instantaneous frequency values is achieved, without leading to mode-mixing issues.

As a comparison with literature methods for adaptive signal decomposition, both the EMD and its multivariate extension, the MEMD, were considered. In particular, the EMD was applied to the time history collected at the location S4 (see Fig. 2), while the MEMD was used to decompose the multivariate signal into four sets of IMFs (one for sensor location). The instantaneous frequencies obtained by applying the HT on the IMFs related to location S4 obtained by means of traditional and multivariate EMD are reported in Fig. 10. Here, the same median filter used to obtain the identified values reported in Fig. 9 is employed. It is possible to notice how the IMFs extracted by EMD are saturated with noise, showing scattered frequencies with a slightly variable mean trend, which are however not able to follow the theoretical curves. On the other hand, MEMD has shown to be less sensitive to noise, exhibiting however strong mode-mixing issues. It is indeed clearly noticeable how the instantaneous frequencies of all IMFs jump to the upper mode at 700 s and back to the lower at 1400 s.
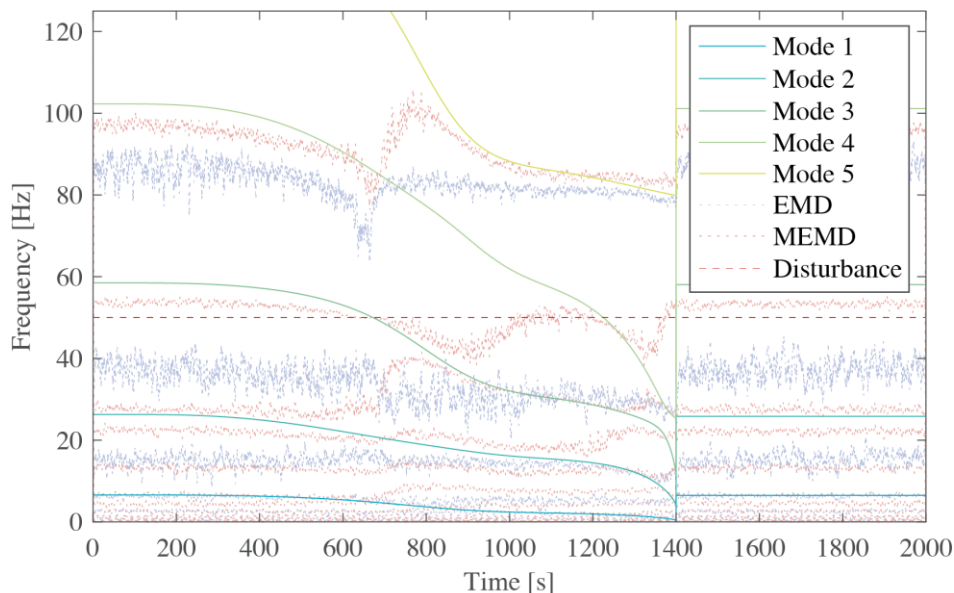

Fig. 10: Instantaneous frequencies estimated through EMD and its multivariate variant

The modal shapes obtained as simple ratios between the modal responses extracted through DAMA are reported in Fig. 11 (the same median filter used for natural frequencies was employed on instantaneous ratios). In particular, the normalization was performed selecting the modal responses of sensor S1 as reference. It is possible to notice how the third mode, which already showed corrupted frequency values close to the intersection with the narrowband disturbance, is also influenced in the modal shape, which exhibits an oscillation across the theoretical curve around 700 s. Moreover, the fifth mode shows reliable estimates only around 800 s, with an underestimation of the ratio elsewhere. The underestimation is also noticeable for mode 4. However, the general and constant shift in the values identified at locations S2, S3, and S4 suggests that the error is only related to the curve associated with sensor S1. Therefore, different

normalization would have shown better results. On the other hand, modes 1 and 2 are identified with a very good approximation, regardless of the noise and narrowband disturbance.
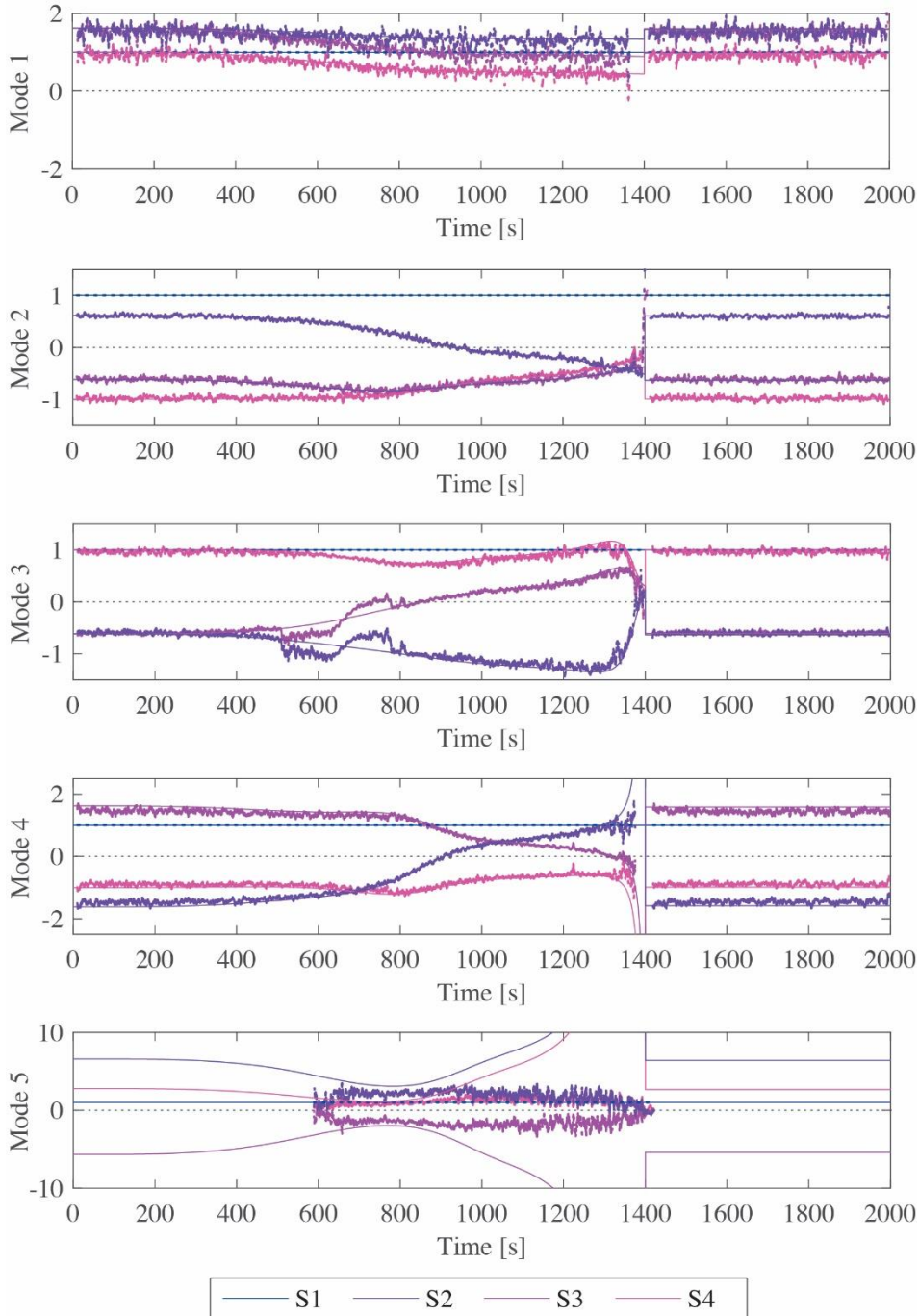

Fig. 11: Theoretical (solid lines) and estimated (dots) instantaneous amplitudes of modal shapes (normalized over the amplitude of S1)

4.2 Case study 2: RC building

The second case study analyzed in this paper is a slice of a full-scale 7-story RC building with cantilever structural walls acting as a lateral force resisting system (Fig. 12). The structure is 20 m high and consists of two perpendicular walls in elevation (i.e., web and flange walls) with a horizontal RC slab at each level. In addition, an auxiliary post-tensioned column provides torsional stability and 4 gravity columns support the slabs, as schematized in Fig. 12a.

The test structure was tested on a shaking table at the University of California, San Diego, through the George E. Brown Jr. Network for Earthquake Engineering Simulation program [62–64] under seismic and white noise base-impressed excitation, the second with 0.03g root mean square (RMS) amplitude, as well as under ambient vibration (i.e., with the shaking table locked).
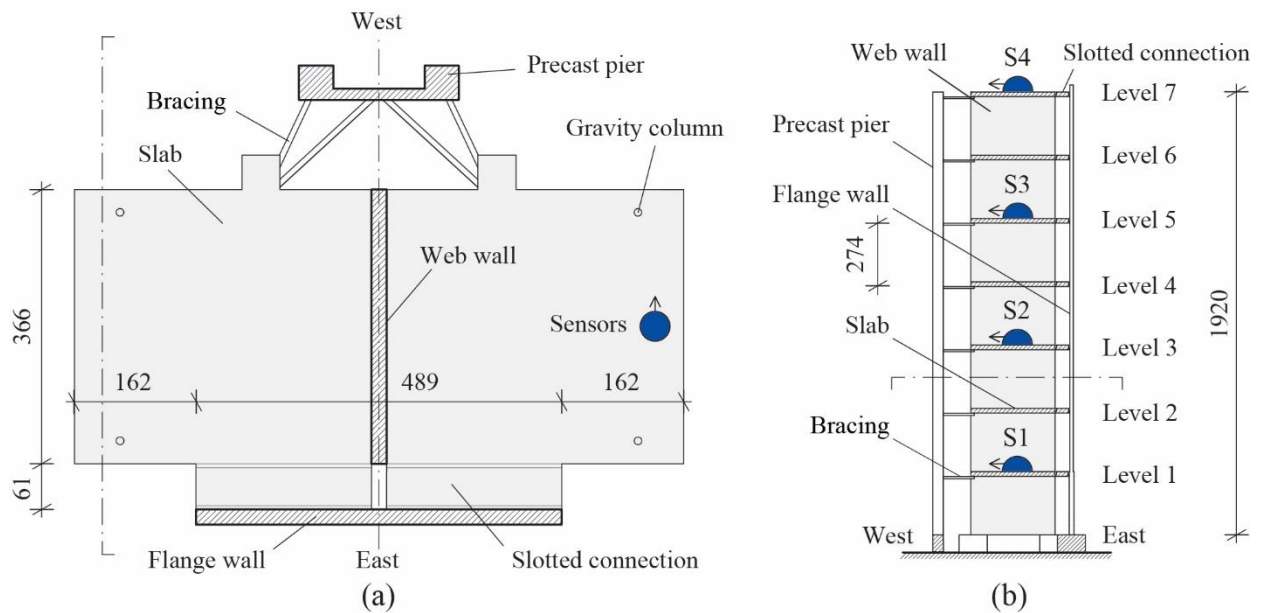

Fig. 12: Case study 2 [64]

The forced vibration tests were designed to progressively damage the building through the simulation of four historical earthquakes of increasing intensity recorded in Southern California. Before and after each test with seismic excitation, the building was subjected to intervals of white noise excitation and ambient vibration. In this paper, only the acceleration collected during the "inspection" intervals after the application of each seismic motion were used. In particular, for the "undamaged" (U) and for each damaged condition (A, B, C, and D), 8 minutes of white noise excitation and 2 minutes of ambient vibration data are considered and merged together in a single set of data with a total duration of 3000 s (as shown in Fig. 13). Therefore, the first 10 minutes of the data set refer to the reference condition U, after which the first seismic excitation (EQ1) of low intensity was applied, consisting of the longitudinal component recorded from the Van Nuys station during the San Fernando earthquake of 1971. Afterward, another inspection interval of 10 minutes is considered, referring to the damaged condition A. The third interval (B) is collected after applying the first medium-intensity seismic excitation EQ2, selected as the transverse component recorded during the San Fernando earthquake from the Van Nuys station in 1971. Interval C was recorded after the second medium-intensity earthquake (EQ3), taken as the longitudinal component of the Northridge earthquake recorded from the Woodland Hills Oxnard Boulevard station in 1994. The last inspection interval (D) was recorded after a high-intensity

360° excitation (EQ4) recorded from the Sylmar Olive View Med during the Northridge earthquake of 1994.

The structure was instrumented with a dense network of sensors with a total of 45 channels: 29 longitudinal (three on each floor slab, one on the web wall at mid-height of each level, and one on the pedestal base), 14 transversal (2 on each floor slab), and 2 vertical (at the base, on the pedestal). The original data is sampled at 240 Hz. More details about the geometry and the instrumentation used can be found in [63–65]. In [63], the results of modal identification obtained by means of different input-output and output-only methods are reported. Here, considering the white noise base excitation, in the undamaged condition, three lateral modes are identified with natural frequencies 1.72 Hz, 11.88 Hz, and 24.64 Hz, respectively. One torsional and one coupled lateral-torsional modes are also identified by some techniques and only during particular damage conditions. Moreover, the MAC values calculated between modal shapes identified through different techniques for these two modes are rather low, showing high level of uncertainties. As shown in [63], indeed, the first lateral mode has a strongly predominant contribution to the total response, making the identification of the torsional mode difficult as it may be covered by the former. In this work, 4 acceleration channels at the locations indicated in Fig. 12 were used (i.e., only longitudinal, at the levels 1, 3, 5, and 7), resampled at 100 Hz, with the intent of identifying the first lateral modes (in the east-west direction) using limited instrumentation.

The Fejér-Korovkin 22 wavelet function with a level 8 was employed for decomposition, generating 256 components with the same frequency range as the previous case study. In this section, the instantaneous natural frequencies and modal responses are estimated by using the output of DAMA and compared with the results reported in [63] regarding the EFDD method, assumed as reference values.
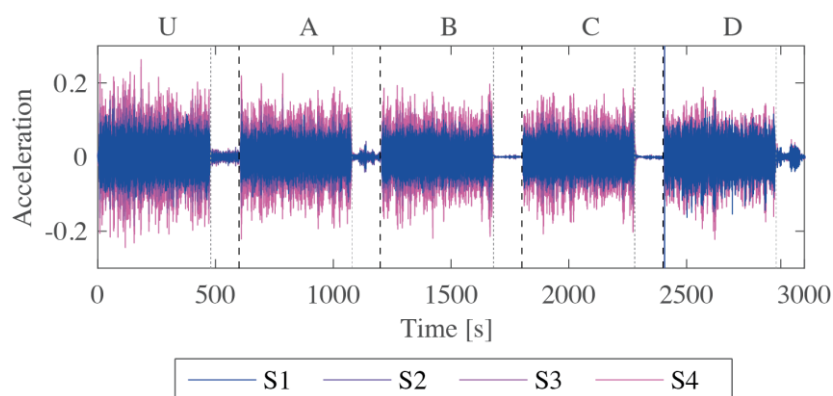

Fig. 13: Multivariate signal used for the second case study

In Fig. 14a, the MAD with a forgetting factor 0.9 is reported. It is possible to notice that high-valued areas are widespread throughout the distribution, making it difficult to recognize different modal responses. The noise-assisted variant presented in Section 3.3 considering 100 trials in the ensemble of noise-added signals (Fig. 14b) was also applied. In this analysis, a set of signal-adaptive Gaussian white noise sequences with standard deviation factor $\beta = 0.3$ was used, with reference to Equation (14). In Fig. 15, the residual variance is represented as a function of the threshold η both for the original formulation (dashed lines) and for the noise-assisted variant (solid lines). It is observable that the first interval characterized by a high slope is more prominent in the result of the noise-assisted procedure, related to the fact that the lower value of MAD for noise-

only areas has shifted around 0.25. It is also noticeable that in the averaged MAD, the areas associated with the first three modal responses are more easily detectable than in the original distribution. Moreover, especially for conditions U and A, high values of MAD are obtained also for the signal parts recorded under low-amplitude ambient vibration, allowing the extraction of modal responses even when the signal amplitude is very low since MAD is not based on the energy distribution in the time-frequency plane as for traditional TFRs. In particular, as concerns the ambient vibration recordings of conditions B, C, and D, narrower areas are detected, the values of which are however close to 1, as in the white noise excitation counterparts. In other words, the extraction of high-value areas in the MAD allows the extraction of modal responses regardless of the signal amplitude, making the method suitable also for non-stationary recordings.

The red areas shown in Fig. 14c represent the result of watershed segmentation applied to the masked MAD distribution, obtained by setting a threshold $\eta = 0.5$. After applying the MAC-based clustering with $\theta = 0.05$ on the partial reconstructed signals, the resulting decomposition is represented in Fig. 14d. Thus, three modal responses are identified, which can be extracted by merging the related partial reconstructed signals.
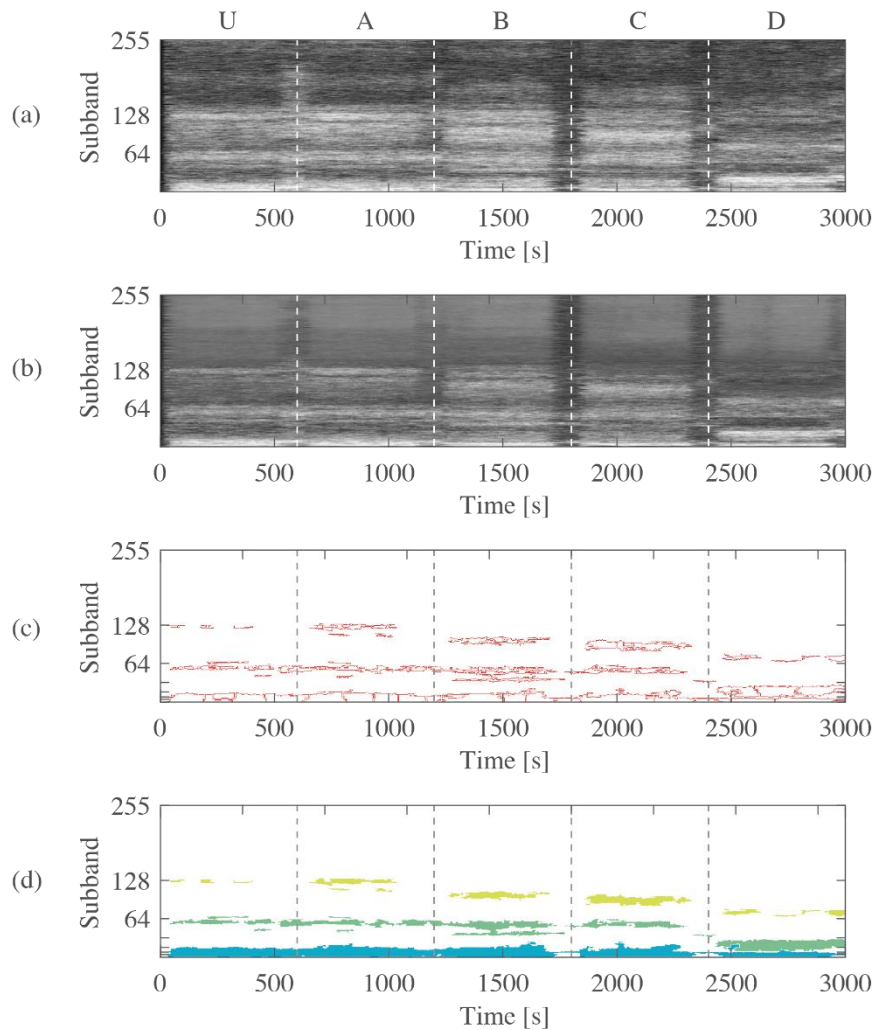

Fig. 14: Smoothed MAD, noise-assisted MAD, watershed segmentation and DAMA application
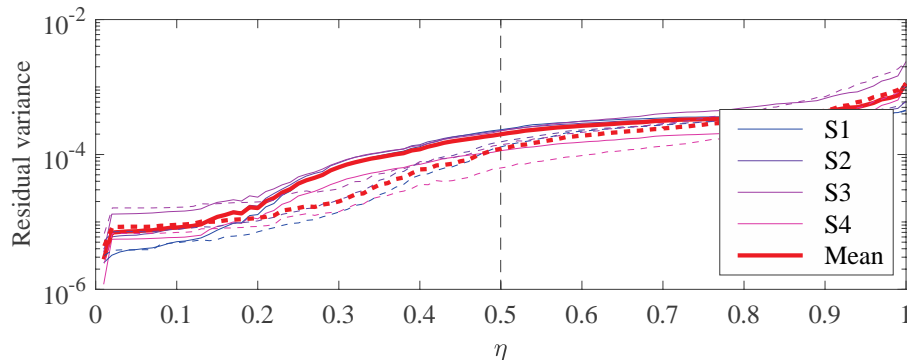
Fig. 15: Residual variance for different values of threshold, case study 2; solid lines indicate the results of the noise-assisted method, while dashed lines indicate the use of forgetting factor only

After extracting the decoupled modal responses, the instantaneous frequencies (calculated using the modal responses extracted at level 7) are estimated through the HT and reported in Fig. 16. Identified instantaneous values are superimposed on the reference estimates obtained in [63] through EFDD, represented as constant values over each condition. Due to system non-linearities, a significant shift in natural frequency is observable within the same condition when passing from a higher-amplitude white noise excitation to ambient vibration. While the instantaneous frequency of mode 1 is almost perfectly reconstructed, also tracking the shifts due to non-linearity, a higher variability in identified values is notable for the higher modes. This fact may be due to the presence of a combined lateral-torsional mode in the frequency band between 7 and 12 Hz [63], the shapes of which are classified as "similar" to the shapes of the identified translational modes since only four acceleration channels are considered in this study to evaluate the MAC. This phenomenon can be observed for mode 2 in condition B, where two neighboring high-valued areas in the MAD are assigned to the same mode during the clustering process (Fig. 14d), although they are well separated in the time-frequency distribution.
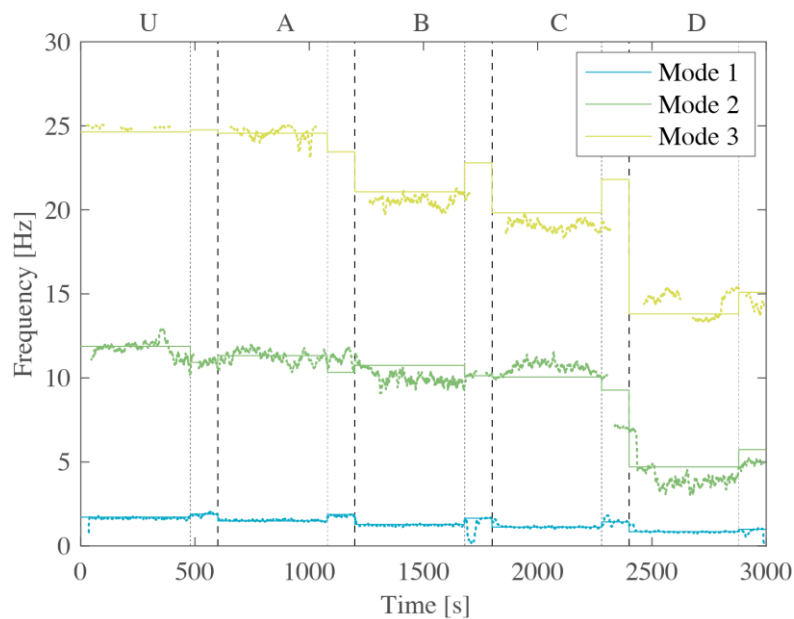

Fig. 16: Theoretical (solid lines) and estimated (dots) instantaneous natural frequencies

22

The uncertainties related to the second mode are also visible in the instantaneous estimate of the related modal shape (Fig. 17), which is generally more dispersed with respect to those of modes 1 and 3. On the right side of Fig. 17, the average modal shapes evaluated over each damage condition are reported, with the color changing from green to red as the damage increases. For modes 1 and 3, an increment in the displacement of the first level with damage is noticeable. As regards mode 2, the parameters estimated by sensor 1 are unstable, indicating that the instantaneous ratio between the modal response obtained by sensor 4 and that of sensor 1 varies considerably over time. This phenomenon could be due both to noisy measurements and multicomponent responses. To confirm this fact, a PCA is conducted considering the modal responses extracted at all sensor locations in each damage scenario, the results of which are reported in Fig. 18. In the lower-right part of each diagram, the variance explained by each PC is reported for each mode. High values in the first PC and low values for the other PCs denote mono-component and low-noise responses, meaning that MAD areas have been properly clustered into separate modal responses. On the other hand, low values in the first PC represent noisy recordings or signals containing the information of two or more modal responses. Observing the parameters reported in Fig. 18, the large variance obtained for modes 1 and 3 in the first PC denotes a good accuracy in the extraction of the first modal response. However, considering the values calculated for mode 2, especially for the conditions U, A, and B, the extracted modal response seems to be multi-component. This property also appears in the diagram of the component scores (represented as points in Fig 18), which are sparse in the plane of the first two principal components for mode 2, especially for condition B.

However, observing the principal directions, represented as lines starting from the origin in Fig. 18, it is possible to notice how their projections on the PC 1 axis (interpretable as an estimate of modal shapes) are generally stable, i.e., change slightly as damage increases, except for the direction of sensor S1 for mode 2 which varies considerably in each diagram.
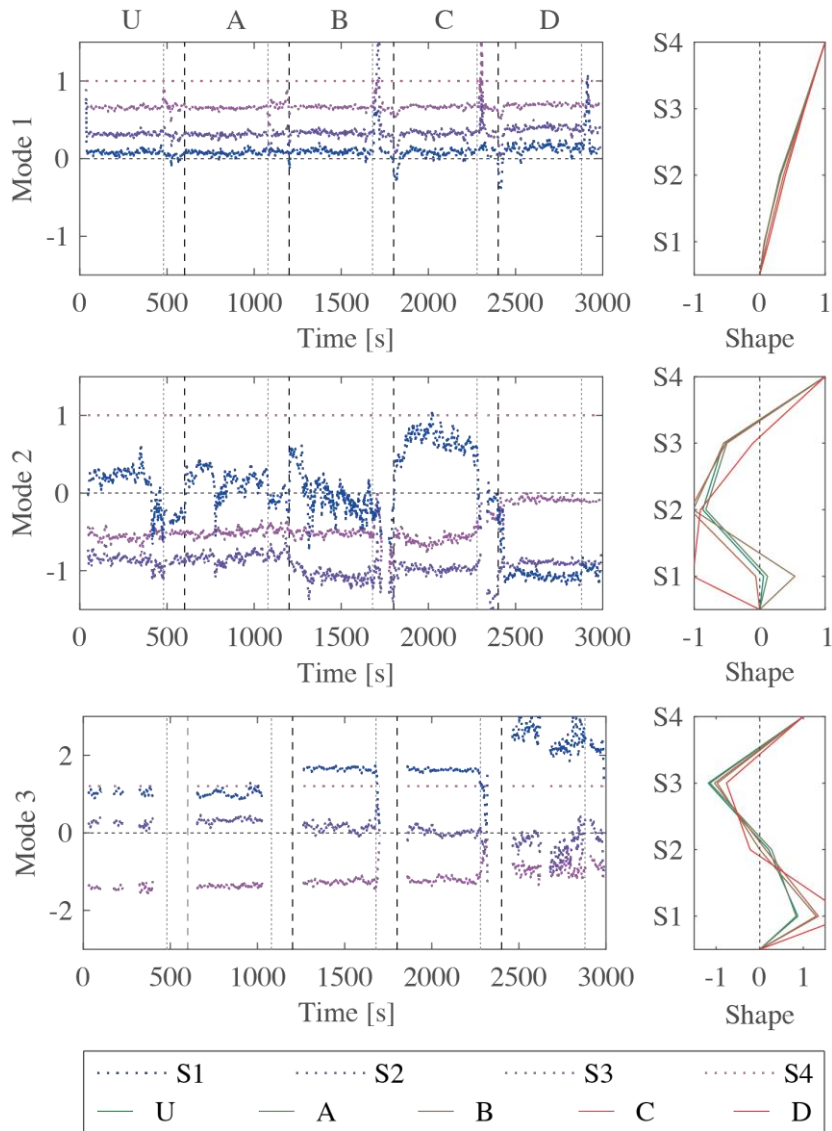
Fig. 17: Instantaneous amplitudes (normalized over the amplitude of S4) of the identified modal shapes (left) and average values for each damage scenario (right)
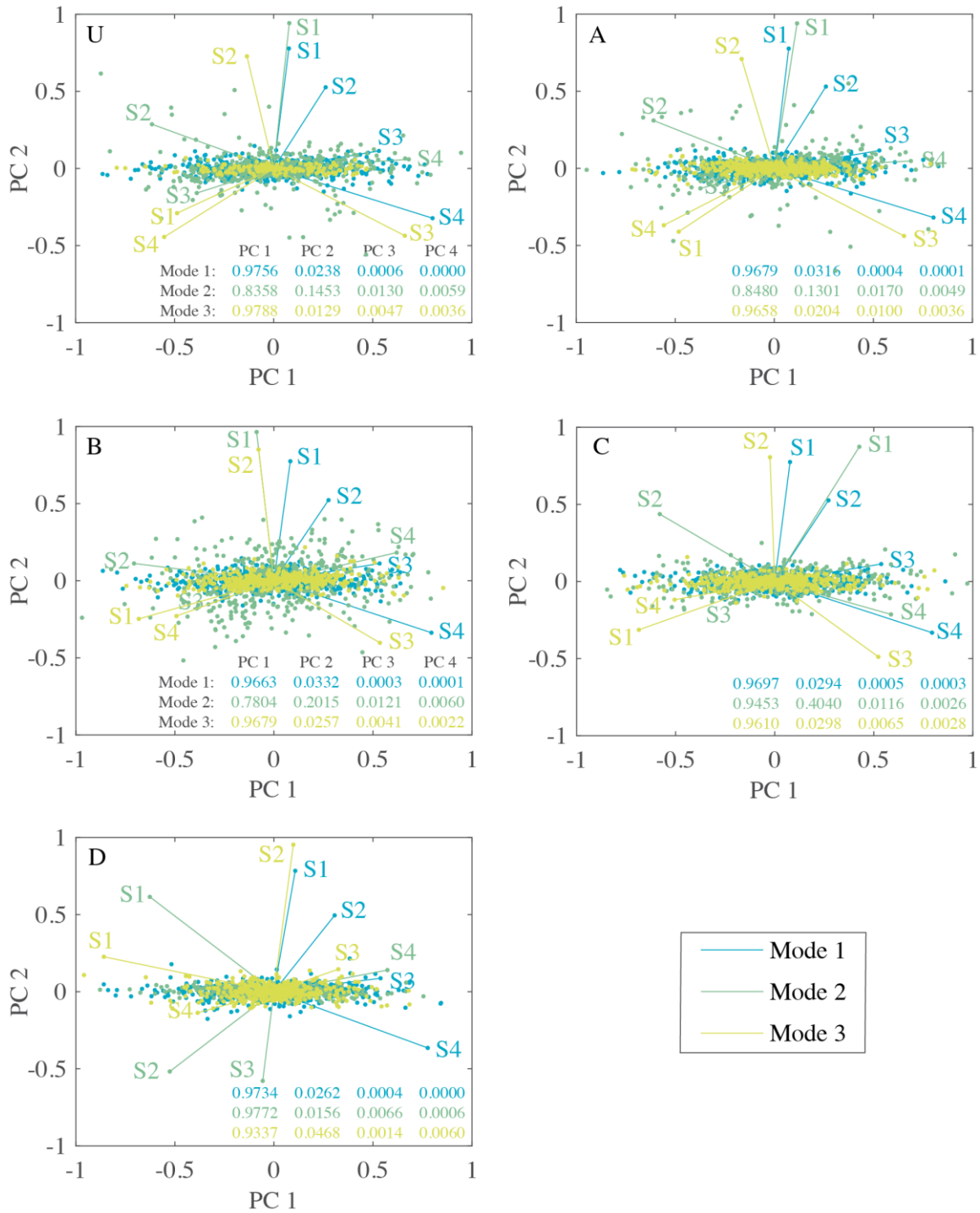
Fig. 18: Principal directions and scores (represented as the first two PCs) of modal responses extracted from white noise recordings for each condition; the numbers on the lower-right part of each diagram represent the percentage of variance explained by each PC

Since a high variability in both instantaneous amplitude and principal direction is observed in conditions U, A, and B only for mode 2 at sensor location S1, the estimation error seems to be related to a low SNR in the frequency band of the second mode for the recording collected at the

first level. In condition D, since considerable damage was experienced [63], the amplitude of the second mode at the location of sensor S1 increased, thus reducing the issues due to the low SNR. According to [63], the higher estimation error of the second lateral mode may also be due to the proximity of its natural frequency to the frequency of the oil column of the vibration table.

It is also observable that the instantaneous estimates of modal shapes are corrupted when passing from a damage scenario to another, as well as when the input excitation changes. This fact may be due to two phenomena. The first regards the delay in the masking matrix due to the forgetting factor adopted to improve the MAD readability. The reconstructed signal is indeed obtained through a bandpass filter which is adapted to the signal with a delay, which could be estimated as illustrated in [44]. The second reason is related to the assumption of slowly varying features, which is violated when a sudden change in the dynamics occurs, i.e., when passing through recordings collected during different inspection intervals.

For comparison, the instantaneous natural frequencies were also extracted by using the HT on IMFs obtained through EMD, EEMD, and MEMD. In Fig. 19, the estimated frequencies are represented superimposed on the reference values. In particular EMD and EEMD were applied on the signal collected by sensor S4, while MEMD considered the four channels used in the previous analyses. It is possible to observe that, although the same median filter used to obtain the values reported in Fig. 16 is used, the identified values are considerably noisier in this case. Moreover, a high number of IMFs is generally extracted, not reflecting the real modal responses and showing mode mixing problems.
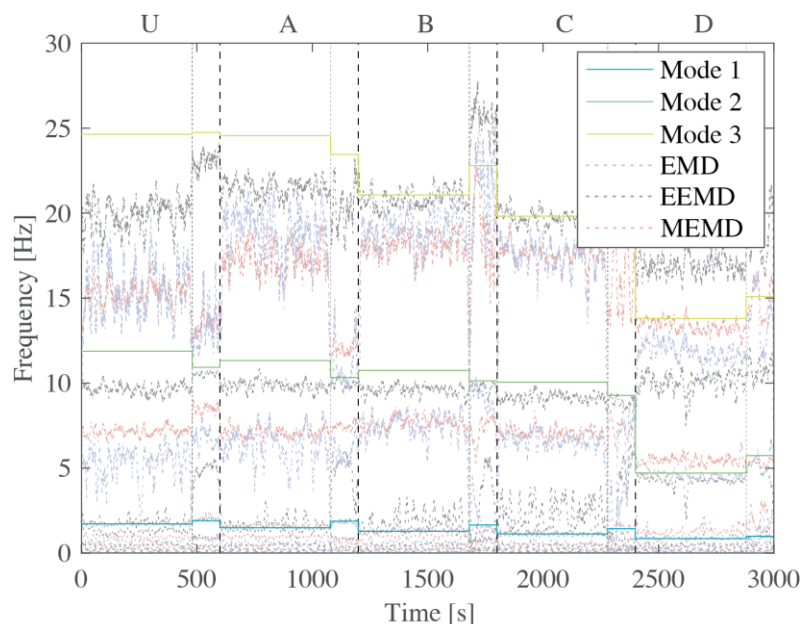

Fig. 19: Instantaneous frequencies estimated through EMD and its variants

5. CONCLUSIONS

In this paper, a novel TFR for multivariate signals is presented, which is not based on the distribution of energy density through the time-frequency plane, but on the similarities between instantaneous ODSs related to neighboring narrow-frequency band signal components. In this

work, the decomposition into signal subbands is performed by means of the discrete WPT, which can be implemented in efficient algorithms for near-real-time applications. In order to improve the readability of MAD, which generally presents random similarities in non-modal ODSs, two criteria are also presented. The first simply involves the use of a forgetting factor, while the second consists of a noise-assisted procedure, which however does not corrupt the final results, as it happens instead in the EEMD if the number of trials is low since noise is only used to create a mask for the extracted signal.

Moreover, the DAMA has been proposed to extract decoupled modal responses by applying a MAD-driven watershed segmentation and a MAC-based clustering procedure. The MAD has shown to be particularly suitable for watershed segmentation, as the areas associated with different modes are well-separated by low values in the distribution. However, the use of a forgetting factor in the MAD may lead to local unreliable estimates of modal parameters, which are nevertheless limited to the intervals where dynamics vary abruptly. The two main parameters of the DAMA have been discussed, also proposing a selection criterion based upon the analyzed signal.

In the Applications section, the theory illustrated in the first part of the paper has been applied to two case studies presenting both slow and abrupt variations in the dynamics. In particular, the analyses conducted on a first simulated case study demonstrate the potential of the method, showing low sensitivity to narrow-band disturbances and performing well also with vanishing modes and considerable variations of the dynamic features. On the other hand, the analyses conducted on the second case study show the applicability of the method to signals collected on real structures, even under varying excitation with non-stationary amplitude. Accurate results are obtained for both the case studies, especially for the lower modes, both in terms of identified instantaneous natural frequencies and modal shapes.

The method proposed is compared with the EMD and its multivariate variant, which has however shown mode mixing problems and the inability to identify vanishing modes. The quality of extracted modal responses was also investigated, attributing the discrepancies between estimated modal parameters and the ones considered as a reference to the presence of noise and imperfect clustering, which may generate multi-component responses.

The idea of measuring the similarity in neighboring ODSs has already been successfully used in the EFDD algorithm for frequency-domain modal identification and is here extended in the time-frequency domain, giving rise to a new adaptive TFR which can be employed as the starting point of several algorithms for signal analysis and system identification, even for near real-time applications.

ACKNOWLEDGEMENTS

REFERENCES

[1]   W. Fan, P. Qiao, Vibration-based damage identification methods: A review and

comparative study, Structural Health Monitoring. 10 (2011) 83–111. https://doi.org/10.1177/1475921710365419.

[2]   M.G. Masciotta, L.F. Ramos, P.B. Lourenço, The importance of structural monitoring as a diagnosis and control tool in the restoration process of heritage structures: A case study in Portugal, Journal of Cultural Heritage. 27 (2017) 36–47. https://doi.org/10.1016/j.culher.2017.04.003.

[3]   M.P. Limongelli, M. Dolce, D. Spina, P. Guéguen, M. Langlais, D. Wolinieck, E. Maufroy, C.Z. Karakostas, V.A. Lekidis, K. Morfidis, T. Salonikios, E. Rovithis, K. Makra, M.G. Masciotta, P.B. Lourenço, S 2 HM in some European countries, Springer Tracts in Civil Engineering. (2019) 303–343. https://doi.org/10.1007/978-3-030-13976-6_13.

[4]   R. Uma Maheswari, R. Umamaheswari, Trends in non-stationary signal processing techniques applied to vibration analysis of wind turbine drive train – A contemporary survey, Mechanical Systems and Signal Processing. 85 (2017) 296–311. https://doi.org/10.1016/j.ymssp.2016.07.046.

[5]   W. Qiao, D. Lu, A Survey on Wind Turbine Condition Monitoring and Fault Diagnosis - Part II: Signals and Signal Processing Methods, IEEE Transactions on Industrial Electronics. 62 (2015) 6546–6557. https://doi.org/10.1109/TIE.2015.2422394.

[6]   S.D. Fassois, J.S. Sakellariou, Time-series methods for fault detection and identification in vibrating structures, Philosophical Transactions of the Royal Society A: Mathematical, Physical and Engineering Sciences. 365 (2007) 411–448. https://doi.org/10.1098/rsta.2006.1929.

[7]   C. Smith, C.M. Akujuobi, P. Hamory, K. Kloesel, An approach to vibration analysis using wavelets in an application of aircraft health monitoring, Mechanical Systems and Signal Processing. 21 (2007) 1255–1272. https://doi.org/10.1016/j.ymssp.2006.06.008.

[8]   M.P. Limongelli, Z.I. Turksezer, P.F. Giordano, Structural health monitoring for cultural heritage constructions: A resilience perspective, IABSE Symposium, Guimaraes 2019: Towards a Resilient Built Environment Risk and Asset Management - Report. (2019) 1552–1559.

[9]   M.D. Spiridonakos, S.D. Fassois, Parametric identification of a time-varying structure based on vector vibration response measurements, Mechanical Systems and Signal Processing. 23 (2009) 2029–2048. https://doi.org/10.1016/j.ymssp.2008.11.004.

[10]   M.S. Allen, M.W. Sracic, S. Chauhan, M.H. Hansen, Output-only modal analysis of linear time-periodic systems with application to wind turbine simulation data, Mechanical Systems and Signal Processing. 25 (2011) 1174–1191. https://doi.org/10.1016/j.ymssp.2010.12.018.

[11]   A. Senba, H. Furuya, Implementation algorithms for self-identification of adaptive structures with variable geometric properties, Mechanical Systems and Signal Processing. 22 (2008) 1–14. https://doi.org/10.1016/j.ymssp.2007.05.002.

[12]   Z. Ni, R. Mu, G. Xun, Z. Wu, Time-varying modal parameters identification of a spacecraft with rotating flexible appendage by recursive algorithm, Acta Astronautica. 118 (2016) 49–61. https://doi.org/10.1016/j.actaastro.2015.10.001.

[13]   R. Ditommaso, M. Mucciarelli, F.C. Ponzo, Analysis of non-stationary structural systems by using a band-variable filter, Bulletin of Earthquake Engineering. 10 (2012) 895–911. https://doi.org/10.1007/s10518-012-9338-y.

[14]   R. Ditommaso, F.C. Ponzo, G. Auletta, Damage detection on framed structures: modal curvature evaluation using Stockwell Transform under seismic excitation, Earthquake

Engineering and Engineering Vibration. 14 (2015) 265–274. https://doi.org/10.1007/s11803-015-0022-5.

[15]   C. Iacovino, R. Ditommaso, F.C. Ponzo, M.P. Limongelli, The Interpolation Evolution Method for damage localization in structures under seismic excitation, Earthquake Engineering and Structural Dynamics. 47 (2018) 2117–2136. https://doi.org/10.1002/eqe.3062.

[16]   A.G. Poulimenos, S.D. Fassois, Parametric time-domain methods for non-stationary random vibration modelling and analysis - A critical survey and comparison, Mechanical Systems and Signal Processing. 20 (2006) 763–816. https://doi.org/10.1016/j.ymssp.2005.10.003.

[17]   M.D. Spiridonakos, S.D. Fassois, Adaptable functional series TARMA models for non-stationary signal modelling, IFAC, 2012. https://doi.org/10.3182/20120711-3-BE-2027.00200.

[18]   M. Vetterli, J. Kovačević, Wavelets and Subband Coding, 1995.

[19]   D. Gabor, Theory of communication. Part 1: The analysis of information, Journal of the Institution of Electrical Engineers - Part III: Radio and Communication Engineering. 93 (1946) 429–441. https://doi.org/10.1049/ji-3-2.1946.0074.

[20]   I. Daubechies, Ten Lectures on Wavelets, 1992. https://doi.org/10.1137/1.9781611970104.

[21]   R.G. Stockwell, Localization of the complex spectrum: the s transform, IEEE Transactions on Signal Processing. 44 (1996) 993. https://doi.org/10.1109/78.492555.

[22]   L. Cohen, Time Frequency Analysis: Theory and Applications, (1995) 299.

[23]   B. Boashash, Theory of Quadratic TFDs, Time Frequency Analysis: A Comprehensive Reference. (2003) 59–81. https://doi.org/10.1016/B978-008044335-5/50024-3.

[24]   F. Auger, P. Flandrin, Y. Lin, S. Mclaughlin, T. Oberlin, H. Wu, F. Auger, P. Flandrin, Y. Lin, S. Mclaughlin, S. Meignen, Time-frequency reassignment and synchrosqueezing: An overview, IEEE Signal Processing Magazine. 30 (2014). https://doi.org/10.1109/MSP.2013.2265316.

[25]   I. Daubechies, J. Lu, H.T. Wu, Synchrosqueezed wavelet transforms: An empirical mode decomposition-like tool, Applied and Computational Harmonic Analysis. 30 (2011) 243–261. https://doi.org/10.1016/j.acha.2010.08.002.

[26]   N.E. Huang, Z. Shen, S.R. Long, M.C. Wu, H.H. Snin, Q. Zheng, N.C. Yen, C.C. Tung, H.H. Liu, The empirical mode decomposition and the Hubert spectrum for nonlinear and non-stationary time series analysis, Proceedings of the Royal Society A: Mathematical, Physical and Engineering Sciences. 454 (1998) 903–995. https://doi.org/10.1098/rspa.1998.0193.

[27]   R. Ditommaso, M. Mucciarelli, S. Parolai, M. Picozzi, Monitoring the structural dynamic response of a masonry tower: Comparing classical and time-frequency analyses, Bulletin of Earthquake Engineering. 10 (2012) 1221–1235. https://doi.org/10.1007/s10518-012-9347-x.

[28]   Z. Wu, N.E. Huang, Ensemble empirical mode decomposition: A noise-assisted data analysis method, Advances in Adaptive Data Analysis. 1 (2009) 1–41. https://doi.org/10.1142/S1793536909000047.

[29]   J.M. Lilly, S.C. Olhede, Analysis of modulated multivariate oscillations, IEEE Transactions on Signal Processing. 60 (2012) 600–612. https://doi.org/10.1109/TSP.2011.2173681.

[30]   A. Omidvarnia, B. Boashash, G. Azemi, P. Colditz, S. Vanhatalo, Generalised phase

synchrony within multivariate signals: An emerging concept in time-frequency analysis, ICASSP, IEEE International Conference on Acoustics, Speech and Signal Processing - Proceedings. (2012) 3417–3420. https://doi.org/10.1109/ICASSP.2012.6288650.

[31] L. Stanković, D. Mandić, M. Daković, M. Brajović, Time-frequency decomposition of multivariate multicomponent signals, Signal Processing. 142 (2018) 468–479. https://doi.org/10.1016/j.sigpro.2017.08.001.

[32] A. Ahrabian, D. Looney, L. Stanković, D.P. Mandic, Synchrosqueezing-based time-frequency analysis of multivariate data, Signal Processing. 106 (2015) 331–341. https://doi.org/10.1016/j.sigpro.2014.08.010.

[33] N. Rehman, D.P. Mandic, Multivariate empirical mode decomposition, Proceedings of the Royal Society A: Mathematical, Physical and Engineering Sciences. 466 (2010) 1291–1302. https://doi.org/10.1098/rspa.2009.0502.

[34] N. Ur Rehman, D.P. Mandic, Filter bank property of multivariate empirical mode decomposition, IEEE Transactions on Signal Processing. 59 (2011) 2421–2426. https://doi.org/10.1109/TSP.2011.2106779.

[35] M.R. Thirumalaisamy, P.J. Ansell, Fast and Adaptive Empirical Mode Decomposition for Multidimensional, Multivariate Signals, IEEE Signal Processing Letters. 25 (2018) 1550–1554. https://doi.org/10.1109/LSP.2018.2867335.

[36] D. Iatsenko, P.V.E. McClintock, A. Stefanovska, Extraction of instantaneous frequencies from ridges in time-frequency representations of signals, Signal Processing. 125 (2016) 290–303. https://doi.org/10.1016/j.sigpro.2016.01.024.

[37] L.E. Avendaño, L.D. Avendaño-Valencia, E. Delgado-Trejos, Diagonal time dependent state space models for modal decomposition of non-stationary signals, Signal Processing. 147 (2018) 208–223. https://doi.org/10.1016/j.sigpro.2018.01.031.

[38] N. Delprat, P. Guillemain, B. Escudie, R. Kronland-Martinet, P. Tchamitchian, B. Torresani, Asymptotic Wavelet and Gabor Analysis: Extraction of Instantaneous Frequencies, IEEE Transactions on Information Theory. 38 (1992) 644–664. https://doi.org/10.1109/18.119728.

[39] L. Rankine, M. Mesbah, B. Boashash, IF estimation for multicomponent signals using image processing techniques in the time-frequency domain, Signal Processing. 87 (2007) 1234–1250. https://doi.org/10.1016/j.sigpro.2006.10.013.

[40] W.J. Staszewski, Identification of non-linear systems using multi-scale ridges and skeletons of the wavelet transform, Journal of Sound and Vibration. 214 (1998) 639–658. https://doi.org/10.1006/jsvi.1998.1616.

[41] C. Wang, W.X. Ren, Z.C. Wang, H.P. Zhu, Instantaneous frequency identification of time-varying structures by continuous wavelet transform, Engineering Structures. 52 (2013) 17–25. https://doi.org/10.1016/j.engstruct.2013.02.006.

[42] N. Özkurt, F.A. Savaci, Determination of Wavelet Ridges of Nonstationary Signals by Singular Value Decomposition, IEEE Transactions on Circuits and Systems II: Express Briefs. 52 (2005) 480–485. https://doi.org/10.1109/TCSII.2005.849041.

[43] T.P. Le, P. Paultre, Modal identification based on the time-frequency domain decomposition of unknown-input dynamic tests, International Journal of Mechanical Sciences. 71 (2013) 41–50. https://doi.org/10.1016/j.ijmecsci.2013.03.005.

[44] S. Quqa, L. Landi, P.P. Diotallevi, Instantaneous modal identification under varying structural characteristics: A decentralized algorithm, Mechanical Systems and Signal Processing. (2020). https://doi.org/10.1016/j.ymssp.2020.106750.

[45] S. Quqa, L. Landi, P.P. Diotallevi, Recursive identification of frequency-amplitude model for damage detection in structures with non-linear behaviour, in: XVIII Conference of the Italian National Association of Earthquake Engineering, Ascoli Piceno, IT, 2019: pp. SG12-50.

[46] S. Quqa, L. Landi, P.P. Diotallevi, Real Time Damage Detection Through Single Low-Cost Smart Sensor, in: Computational Methods in Structural Dynamics and Earthquake Engineering, Crete, GR, 2019: pp. 3914–3925. https://doi.org/10.7712/120119.7196.19614.

[47] W.M. Liu, V.J.R. Bastante, F.R. Rodriguez, N.W.D. Evans, J.S.D. Mason, Morphological filtering of spectrograms for automatic speech recognition, Proceedings of the Fourth IASTED International Conference on Visualization, Imaging, and Image Processing. (2004) 546–549.

[48] S. Gómez, V. Naranjo, R. Miralles, Removing interference components in time-frequency representations using morphological operators, Journal of Visual Communication and Image Representation. 22 (2011) 401–410. https://doi.org/10.1016/j.jvcir.2011.03.007.

[49] Z. Zhang, K. Xu, D. Ta, W. Wang, Joint spectrogram segmentation and ridge-extraction method for separating multimodal guided waves in long bones, Science China: Physics, Mechanics and Astronomy. 56 (2013) 1317–1323. https://doi.org/10.1007/s11433-013-5110-9.

[50] L. Vincent, L. Vincent, P. Soille, Watersheds in Digital Spaces: An Efficient Algorithm Based on Immersion Simulations, IEEE Transactions on Pattern Analysis and Machine Intelligence. 13 (1991) 583–598. https://doi.org/10.1109/34.87344.

[51] A. Roueff, J. Chanussot, J.I. Mars, M.Q. Nguyen, Unsupervised separation of seismic waves using the watershed algorithm on time-scale images, Geophysical Prospecting. 52 (2004) 287–300. https://doi.org/10.1111/j.1365-2478.2004.00416.x.

[52] L. He, X. Ren, Q. Gao, X. Zhao, B. Yao, Y. Chao, The connected-component labeling problem: A review of state-of-the-art algorithms, Pattern Recognition. 70 (2017) 25–43. https://doi.org/10.1016/j.patcog.2017.04.018.

[53] H. Zhuang, B.S. Oh, D. Lin, K.A. Toh, Z. Lin, Multicomponent Signal Decomposition Using Morphological Operations, International Conference on Digital Signal Processing, DSP. 2018-Novem (2019) 1–5. https://doi.org/10.1109/ICDSP.2018.8631863.

[54] P. Soille, Morphological Image Analysis, 2004. https://doi.org/10.1007/978-3-662-05088-0.

[55] R.J. Allemang, The modal assurance criterion - Twenty years of use and abuse, Sound and Vibration. 37 (2003) 14–21.

[56] E. Reynders, R. Pintelon, G. De Roeck, Uncertainty bounds on modal parameters obtained from stochastic subspace identification, Mechanical Systems and Signal Processing. 22 (2008) 948–969. https://doi.org/10.1016/j.ymssp.2007.10.009.

[57] N.-J. Jacobsen, P. Andersen, R. Brincker, Using enhanced frequency domain decomposition as a robust technique to harmonic excitation in operational modal analysis, in: Proceedings of ISMA2006: International Conference on Noise and Vibration Engineering, 2006: pp. 3129–3140.

[58] A.K. Chopra, Dynamics of Structures: Theory and Applications to Earthquake Engineering, Fourth Edi, Pearson, 2017. https://doi.org/9780134555126.

[59] S.G. Mallat, A wavelet tour of signal processing, Third edit, Academic Press, 2009. https://doi.org/10.1016/B978-0-12-374370-1.X0001-8.

[60] G. Strang, T. Nguyen, Wavelets and Filter Banks, SIAM, 1996.

[61] H. Abdi, L.J. Williams, Principal component analysis, Wiley Interdisciplinary Reviews: Computational Statistics. 2 (2010) 433–459. https://doi.org/10.1002/wics.101.

[62] B. Moaveni, X. He, J.P. Conte, J.I. Restrepo, Damage identification study of a seven-story full-scale building slice tested on the UCSD-NEES shake table, Structural Safety. 32 (2010) 347–356. https://doi.org/10.1016/j.strusafe.2010.03.006.

[63] B. Moaveni, X. He, J.P. Conte, J.I. Restrepo, M. Panagiotou, System identification study of a 7-story full-scale building slice tested on the UCSD-NEES shake table, Journal of Structural Engineering. 137 (2011) 705–717. https://doi.org/10.1061/(ASCE)ST.1943-541X.0000300.

[64] P. Martinelli, F.C. Filippou, Simulation of the shaking table test of a seven-story shear wall building, Earthquake Engineering and Structural Dynamics. 38 (2009) 587–607. https://doi.org/10.1002/eqe.897.

[65] B. Moaveni, X. He, J.P. Conte, J.I. Restrepo, Damage identification study of a seven-story full-scale building slice tested on the UCSD-NEES shake table, Structural Safety. 32 (2010) 347–356. https://doi.org/10.1016/j.strusafe.2010.03.006.